

Contents lists available at ScienceDirect

Journal of the Mechanical Behavior of Biomedical Materials

Journal of the Mechanical Behavior of Biomedical Materials

journal homepage: http://www.elsevier.com/locate/jmbbm



Temporal and spatial changes in bone accrual, density, and strain energy density in growing foals

Sara G. Moshage ^a, Annette M. McCoy ^b, John D. Polk ^{c,e,f}, Mariana E. Kersh ^{a,d,*}

- ^a Department of Mechanical Science and Engineering, University of Illinois at Urbana-Champaign, USA
- ^b Department of Veterinary Clinical Medicine, University of Illinois at Urbana-Champaign, USA
- ^c Department of Anthropology, University of Illinois at Urbana-Champaign, USA
- d Beckman Institute for Advanced Science and Technology, University of Illinois at Urbana-Champaign, USA
- ^e Department of Biomedical and Translational Sciences, University of Illinois at Urbana-Champaign, USA
- ^f Department of Kinesiology and Community Health, University of Illinois at Urbana-Champaign, USA

ARTICLE INFO

Keywords: Equine Bone Growth Finite element modeling Strain energy density

ABSTRACT

Bone adaptation is in part driven by mechanical loading, and exercise during youth has been shown to have lifelong benefits for bone health. However, the development of early exercise-based interventions that reduce the incidence of fractures in racing horses is limited by the lack of characterization of normal development in growing bone. Previous efforts to quantify bone development in the horse have relied on repeated radiographs or peripheral quantitative computed tomography scans, which are limited in their assessment of the entire bone. In this study, we acquired computed tomography scans of three Standardbred trotting colts longitudinally between 2 and 12 months of age. Finite-element models were constructed of the left forelimb proximal phalanx and used to assess strain energy density during quiet standing. Growth related changes in mineral density and bone area fraction in the distal epiphysis, mid-diaphysis, and proximal epiphysis were evaluated. Mineral density and bone area fraction uniformly increased in the diaphysis and strain energy density was constant during growth, indicating adaptation to quiet standing. Bone mineral density and bone area fraction increased in the medial quadrant of the proximal epiphysis but not in the fracture-prone lateral quadrant. The data presented provides a benchmark of normal growth trajectories that can be used to evaluate the effect of training regimens during growth.

1. Introduction

Equine fractures that occur during a racing event are often highly publicized, however, 48–78% of fractures have been reported to occur during training (Ely et al., 2009; Verheyen and Wood, 2004). The majority of fatal musculoskeletal injuries in racing horses occur in the metacarpophalangeal (MCP) joint (Parkin et al., 2004b), which experiences the highest joint forces in the distal forelimb (Harrison et al., 2010). The proximal phalanx (P1), a bone in the MCP joint, accounts for approximately 25% of all distal forelimb fractures in racing Thoroughbreds (Verheyen and Wood, 2004) and Standardbreds (Bertuglia et al., 2014). Risk factors for fracture include race length, age, number of previous races/workouts, footing type and condition, and field size (Georgopoulos and Parkin, 2017; Parkin et al., 2004a). Post-mortem

analyses have shown that bone micro-cracks are concentrated in areas of catastrophic fracture, and their prevalence increases with age and increased cyclic loading (Turley et al., 2014; Riggs, 2002). Fatigue fractures, which are thought to be the primary etiology of long-bone fractures in the horse, occur when micro-cracks coalesce and extend (Riggs, 2002). The small length of micro-cracks (approximately $100-500 \ \mu m$) impedes the diagnosis of horses at risk for fatigue fracture using currently available *in vivo* imaging methods (Turley et al., 2014).

Computed tomography (CT) based finite-element analysis, using *in vivo* data, has been used as a predictor of bone strength and strain in both humans and animals (Harrison et al., 2014; Zysset et al., 2013; Kersh et al., 2018). Finite element models of the P1 (Harrison et al., 2014; O'Hare et al., 2013; McCarty et al., 2016) have shown increased stress under galloping loads in locations that are prone to fracture in the

Abbreviations: BA/TA, bone area fraction; CT, computed tomography; FE, finite element; HU, Hounsfield unit; MC3, third metacarpal bone; MCP, metacarpophalangeal joint; P1, proximal phalanx bone; pQCT, peripheral quantitative computed tomography; SED, strain energy density.

^{*} Corresponding author. Department of Mechanical Science and Engineering, University of Illinois at Urbana-Champaign, USA. *E-mail address:* mkersh@illinois.edu (M.E. Kersh).

proximal epiphysis (O'Hare et al., 2013). However, this assessment was performed on a model of an adult P1 bone using material properties obtained from literature and these results may vary in younger horses due to differences in material properties. Further, it is unknown if the stress distribution at a specific gait is constant at different ages or if it changes over time.

Bone fracture risk is a function of the type and orientation of loading in the limbs, and the mechanical strength of the loaded bone (Biewener, 1982; Biewener and Bertram, 1993). Bone quality depends on material properties as well as the structural organization of bone at multiple length scales. During growth, the musculoskeletal system faces the challenge of synergistically regulating muscle and bone properties to accommodate the mechanical demands associated with increasing size and speed. The change in fracture load relative to expected loads in young horses has not been established because of the lack of data on physiological loads. Understanding bone regulation during growth will allow for the identification of critical time points during bone development that may prime bone for modeling or conversely place it at risk of fracture.

Bone functional adaptation is driven, in part, by the mechanical environment (Ruff et al., 2006). Strain levels above the customary threshold leads to bone remodeling and deposition of bone tissue, which acts to reduce the strain to an acceptable level (Frost, 1987). Strain energy density (SED), a measure of the energy required to cause deformation, has been used as a predictor of bone adaptation (Prendergast and Taylor, 1994). Therefore, constant SED during growth suggests adaptation of bone to the increasing loads that accompany increased mass. Exercise increases strain in the bone and may be a method for directing bone remodeling. For example, a relatively short duration of mechanical loading in rat ulnae was shown to enhance the structural properties of bone, leading to increased resistance to fatigue loading (Warden et al., 2005).

Exercise during youth, when bone is highly adaptive to mechanical loads, has been shown to provide life-long improvements in mechanical strength of bone in humans (Warden et al., 2014). Thoroughbred foals exercised 5 days a week for 18 months resulted in increased diaphyseal total cross-sectional area and resistance to bending and torsional deformation in the P1 compared to pasture-exercised control foals (Firth et al., 2011). Additionally, controlled exercise from a young age had beneficial effects on articular chondrocyte viability (Dykgraaf et al., 2008). A subset of the horses went on to train and race as 2- and 3-year-olds. While the overall prevalence and type of orthopedic injuries did not differ between exercised and control horses, the exercised group tended to develop orthopedic injuries later than their control counterparts (Rogers et al., 2008). Thus, existing evidence suggests that early exercise may be beneficial for equine athletes. However, before exercise can be used as a targeted intervention to direct bone growth in a manner that could prevent future injury, it is necessary to understand normal growth and adaptation. Measurements of morphological and compositional changes, and their link to the mechanical state of bone, have not been developed for the fracture-prone P1.

The objective of this study was to characterize how the equine proximal phalanx (P1) adapts to changing loads during growth through the use of longitudinal CT scans throughout the first year of life. Previous work to characterize growth of the P1 in young horses has relied on xeroradiographs (Smallwood et al., 1989) and radiographs (Strand et al., 2007) to qualitatively assess bone shape and structure, and quantitatively characterize closure of the proximal growth plate. Other studies have used peripheral quantitative computed tomography (pQCT) to measure growth, but these data were limited to 2 mm thick scan slices in the diaphysis of the bone (Firth et al., 2011). To the best of our knowledge, there is no longitudinal CT data of the P1 during growth. Therefore, our aims were to (1) measure structure and composition changes in the P1, and (2) calculate SED in the P1 under standing loads to assess the degree of mechanical adaptation during growth.

2. Materials and methods

2.1. Subjects

All protocols were approved by the Institutional Animal Care and Use Committee at University of Illinois at Urbana-Champaign (UIUC). Computed tomography (CT) scans of the distal forelimbs were obtained for 3 male, trotting Standardbred foals that were free of lameness. All foals were born at the UIUC Horse Farm and raised at pasture. Scans were collected from 8 weeks to approximately 1 year of age: Foal 1 (F1) at 11, 19, 28, 36, 47, and 57 weeks; Foal 2 (F2) at 9, 14, 17, 21, 25, 33, 41, and 53 weeks; Foal 3 (F3) at 7, 12, 16, 19, and 24 weeks (Fig. 1A).

2.2. Imaging

During all imaging sessions, subjects were anesthetized (sedation with xylazine and butorphanol, induction with ketamine and midazolam, maintenance on isofluorane or total intravenous anesthesia [midazolam-ketamine-xylazine and/or propofol]) and monitored. Distal forelimbs were scanned in the transverse plane at 120 kVp, 50 cm field of view, and 512 \times 512 matrix size on a LightSpeed-16 CT unit (GE Medical Systems) (Fig. 1B). Nominal voxel dimensions were 0.76±0.15 mm in-plane with depths of 0.66±0.15 mm. Hydroxyapatite phantoms (CIRS Inc) of density 0, 25, 100, 500, and 750 $\it mg/cm^3$ were included in all scans.

2.3. Bone properties

The CT images were aligned such that the sagittal groove of the P1 was vertical in the image (Fiji, Schindelin et al. (2012)). For each timepoint, Hounsfield units (HU) within the scan volume were converted to mineral density using a linear calibration equation obtained from the hydroxyapatite phantoms. Next, the left P1 was semi-automatically segmented (Fig. 1C, Amira 5.6). Cortical and trabecular bone compartments were separated using previously established apparent density (ρ) thresholds (Firth et al., 2011):

$$cortical = \rho \ge 0.71 \ g/cm^3 \tag{1}$$

$$trabecular = 0.28 < \rho < 0.71 \ g/cm^3$$
 (2)

Three regions of interest along the bone were evaluated: the distal and proximal epiphyses, and mid-diaphysis (gray boxes in Fig. 1E). The proximal and distal cross-sections of interest were identified as the section within the epiphysis with the largest total cross-sectional area. The mid-diaphysis (henceforth referred to as "diaphysis") was defined as the location of minimum total cross-sectional area. Cortical and trabecular bone area fraction (BA/TA) and the average apparent mineral density within the cortical and trabecular compartments were calculated. These three regions of interest (proximal, diaphysis, and distal) were further sectioned into functional quadrants (dorsal, medial, lateral, palmar) by identifying the centroid of the cross-section and bisecting the cross-section using lines oriented at 45° and 135° with respect to the dorsal-palmar axis (Fig. 1D). Quadrant-specific values of apparent mineral density and BA/TA were then analyzed. All analyses were performed using custom code (Matlab R2018a, Mathworks, Natick, MA).

2.4. Finite element modeling

Subject-specific finite element (FE) models were constructed for each time point (Fig. 1E). Surface models (STL) of the left P1 were smoothed (Geomagic Design X, 3D Systems) and converted to solid models for assembly in a finite element software (Abaqus 6.14, Simulia). Models were seeded globally at a size of 1.2 mm and meshed using quadratic tetrahedral elements (C3D10). Density (ρ) was converted to Young's modulus (E) using a relation (Equation (3)) for equine bone developed

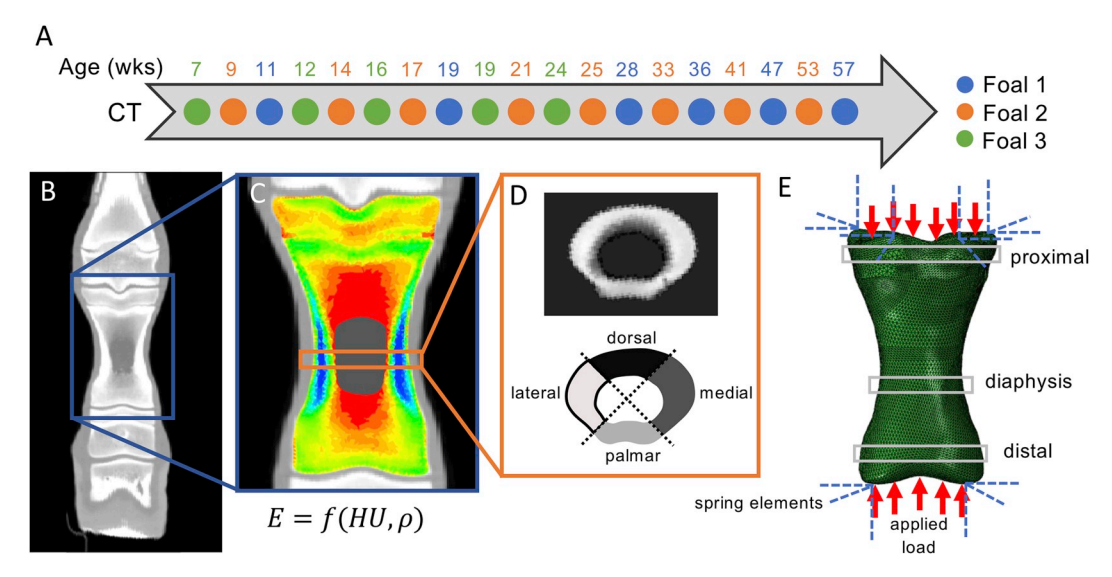


Fig. 1. Development of subject-specific finite-element models and CT scan analysis. (A) Data collected longitudinally for three foals; (B) CT scan of distal left forelimb; (C) proximal phalanx segmented from the scan and Young's modulus shown; (D) example of quadrant analysis, shown for the diaphysis, with a CT cross-section image of the diaphysis shown above a diagram of the quadrants; (E) boundary conditions of the finite-element model, with the three regions of interest (proximal epiphysis, diaphysis, and distal epiphysis) shown in gray boxes.

by Les et al. (1994) and used to assign individual elements modulus values (Bonemat v3.2). All elements were assigned a Poisson's ratio of 0.3.

$$E = 9040\rho^{2.35} \tag{3}$$

Based on prior observations by our group, Standardbred foals between the ages of 2 and 5 months spend more than 80% of their time standing quietly (unpublished data), during which the forelimbs carry approximately 60% of the body weight (Back and Clayton, 2013). Therefore, a compressive load of 30% of body weight times the gravitational constant was applied to the proximal articulating surface of the model of the P1. The load was applied at 145° from the dorsal aspect of the bone, to simulate standing posture (Weller et al., 2006). An equal and opposite load was applied to the distal articulating surface of the bone. Soft tissue constraints were imposed using linear springs applied to the proximal and distal surfaces. Proximal springs had a stiffness of 200 N/mm and distal spring stiffness was 500 N/mm. Stiffness values were chosen to approximate the constraining effects of the superficial digital flexor tendon accessory ligament (Swanstrom et al., 2004), joint congruency, and other soft tissues.

Strain energy density during quiet standing was calculated using a linear implicit analysis. The mean strain energy density for cortical and trabecular bone was calculated at the same cross-sectional regions of interest used for bone property analysis, excluding elements with

mineral density values below the bone threshold (i.e., elements within the marrow cavity).

2.5. Statistical analysis

All statistical analyses were performed in RStudio (R v.3.5.3). Correlations between mass and parameters of interest (strain energy, mineral density, and bone area fraction) were analyzed using linear regressions. Statistical significance of the Pearson's correlation coefficient was assessed at $\alpha=0.05$. Reported values are given as mean \pm standard deviation.

3. Results

3.1. Strain energy density, mineral density, and structure during growth

From seven to fifty-seven weeks of age, mass increased from 120 kg to 382 kg (range of all foals). During this time frame, strain energy density (SED) in cortical bone was highest in the proximal region. SED in both the distal and proximal epiphyses increased with increasing mass (Fig. 2A). Within the distal region, SED in the trabecular bone increased at a rate almost three times that of the cortical bone (6 x 10^{-4} and 2.3 x 10^{-4} ($\mu J/mm^3$)/kg, respectively, Table 1). In the proximal region, SED increased at similar rates in the cortical (4.8 x 10^{-4} ($\mu J/mm^3$)/kg) and

Table 1 Slopes and intercept values for linear regressions used to characterize changes in strain energy density, mineral density, and bone area fraction of cortical and trabecular bone with increasing mass (see Fig. 2). The units for strain energy density (SED) are $\mu J/mm^3$, units of apparent mineral density are $mg~HA/cm^3$, and units of bone area fraction are %.

		Distal		Diaphysis		Proximal	
		cortical	trabecular	cortical	trabecular	cortical	trabecular
Strain Energy Density	slope	2.3 e-4	6.0 e-4	1.7 e-4	3.1 e-5	4.8 e-4	4.9 e-4
	intercept	0.015	0.021	0.03	0.011	0.019	0.0065
	R (p)	0.47 (0.066)	0.7 (0.0016)	0.67 (0.0031)	0.37 (0.14)	0.59 (0.016)	0.58 (0.015)
Mineral Density	slope	0.33	0.26	0.39	-0.078	0.41	0.36
	intercept	760	390	1000	510	670	380
	R (p)	0.48 (0.038)	0.59 (0.0079)	0.38 (0.11)	-0.66 (0.002)	0.66 (0.0019)	0.6 (0.0071)
Bone Area Fraction	slope	0.088	-0.079	0.059	-0.017	0.086	-0.061
	intercept	-12	110	44	21	-12	100
	R (p)	0.68 (0.0014)	-0.65 (0.0024)	0.69 (0.0011)	-0.36 (0.13)	0.59 (0.0085)	-0.46 (0.047)

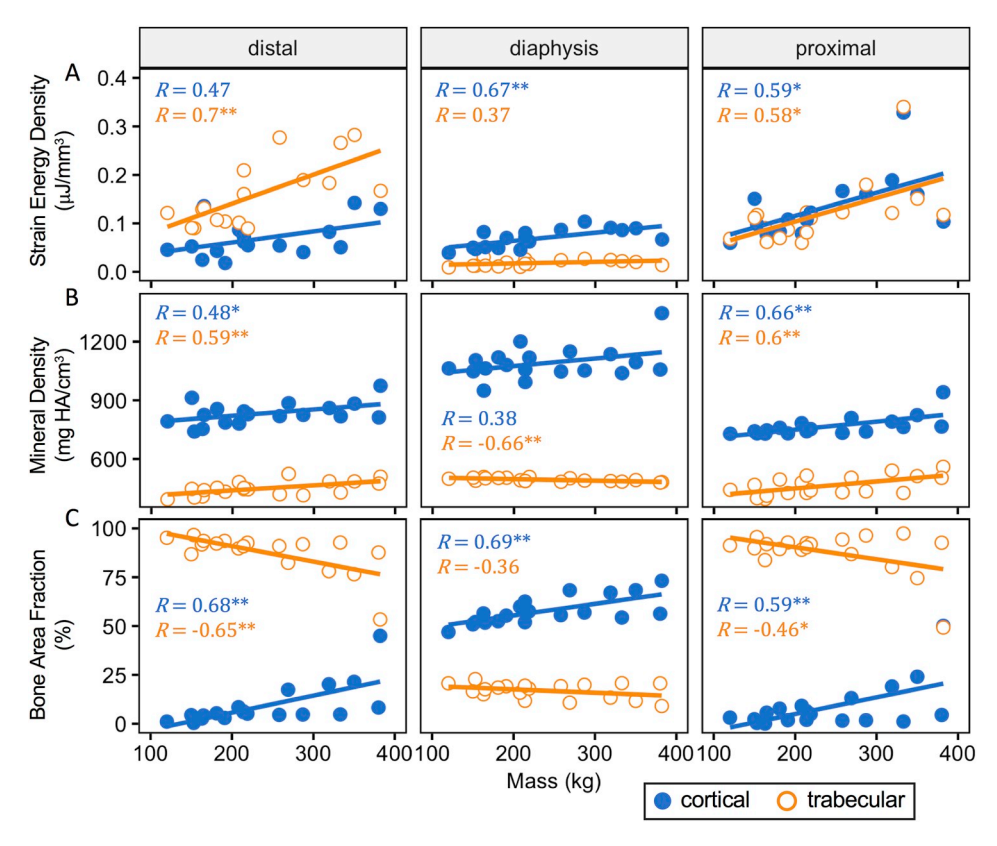


Fig. 2. Properties at cross-sections of interest (distal, diaphysis, and proximal) correlated to increases in mass. (A) Average strain energy density obtained from the subject-specific finite element analysis; (B) average apparent mineral density; (C) bone area fraction (bone area/total area). For all subplots, analysis was divided between cortical bone, indicated by the solid blue circles, and trabecular bone, indicated by the open orange circles. Linear regressions are fit to all foals and ages shown in Fig. 1A. Equations for each linear regression are given in Table 1. For example, the equation for mineral density of cortical bone in the distal epiphysis is y =0.33x + 760, R = 0.48, p = 0.038. The correlation coefficient and accompanying significance value are shown for each line in the subplot. Statistical significance is indicated by the following symbols: p < 0.05, p < 0.01.

trabecular (4.9 x $10^{-4}~(\mu J/mm^3)/kg$) compartments. SED in trabecular bone of the diaphysis was low and nearly constant with increasing mass (1.81 $\pm~0.66~{\rm x}~10^{-2}~\mu J/mm^3$), while there was a minor increase in cortical SED.

Cortical bone in the diaphysis was more dense (1091 \pm 83 $mg\,HA/cm^3$) than in the distal (821 \pm 67 $mg\,HA/cm^3$) and proximal epiphyses (763 \pm 48 $mg\,HA/cm^3$, Fig. 2B). Cortical mineral density increased at similar rates in all three regions (0.33 distal, 0.39 diaphysis, and 0.41

proximal $(mg \, HA \, /cm^3)/kg$, Table 1). The apparent mineral density of trabecular bone increased in the distal and proximal regions (0.26 and 0.36 $(mg \, HA \, /cm^3)/kg$, respectively) and decreased within the diaphysis ($-0.078 \, (mg \, HA \, /cm^3)/kg$).

Cortical area fraction in the diaphysis was higher (57.0 \pm 7.2%) than cortical area fraction in the distal (7.87 \pm 10.0%) and proximal (7.57 \pm 11.1%) epiphyses (Fig. 2C)). Changes in bone area fraction with increasing mass for cortical and trabecular bone in the distal and

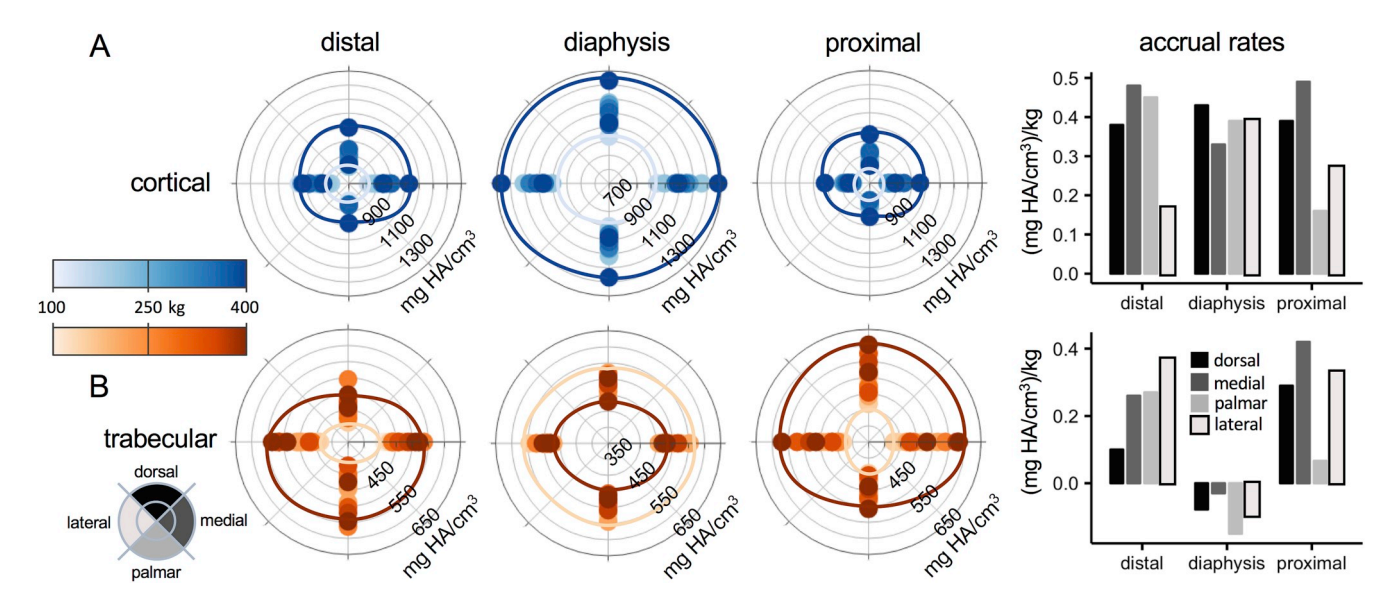


Fig. 3. Apparent mineral density in quadrants of the proximal phalanx for (A) cortical and (B) trabecular bone. Density in $mg \, HA/cm^3$ is plotted on the radial axis of the polar plots. Blue points represent cortical data, while orange points represent trabecular data. The lightly shaded lines indicate the data at 120 kg, while the darker shaded lines indicate the data at 382 kg. Evaluating the gap between these lines gives one an idea of growth in specific quadrants. Bar plots represent the accrual rates (change in density/change in mass) for each quadrant and region. Columns are (left to right): distal epiphysis, diaphysis, proximal epiphysis, accrual rates.

proximal epiphyses were similar. Cortical area fraction increased (0.088 and 0.086 %/kg, distal and proximal, respectively, Table 1) while trabecular area fraction decreased (-0.079 and -0.061 %/kg, distal and proximal).

3.2. Changes in density and structure in anatomical quadrants

Cortical mineral density in the distal and proximal epiphyses increased fastest in the medial quadrant, at 0.48 and 0.49 $(mg\,HA/cm^3)/kg$, respectively (Fig. 3A). The epiphyses had similar cortical mineral density accrual rates in the dorsal quadrant, at 0.38 (distal) and 0.39 (proximal) $(mg\,HA/cm^3)/kg$. The diaphysis had similar cortical mineral density accrual rates in all quadrants, spanning 0.33–0.43 $(mg\,HA/cm^3)/kg$. Trabecular mineral density decreased in all quadrants of the diaphysis, and increased most rapidly in the medial quadrant of the proximal epiphysis (0.42 $(mg\,HA/cm^3)/kg$, Fig. 3B). Trabecular density increased most in the lateral quadrant of the distal epiphysis (0.37 $(mg\,HA/cm^3)/kg$).

Cortical BA/TA accrued at a uniform rate in all quadrants of the diaphysis (Fig. 4A), ranging from 0.056 - 0.066%/kg. Most changes in cortical and trabecular BA/TA in the proximal epiphysis occurred in the dorsal and medial quadrants. Cortical bone accrued at a rate of 0.11 and 0.15%/kg (dorsal and medial, respectively) while trabecular bone area decreased by -0.11 and -0.12%/kg. Increases in distal epiphyseal cortical bone area fraction were matched by equal decreases in trabecular bone area fraction accrual (Fig. 4B). Within the distal epiphysis, most change in both cortical and trabecular bone area fraction accrual occurred in the medial quadrant.

4. Discussion

Using subject-specific models of the P1 during growth, we found that the diaphysis of the P1 adapts to quiet standing as evidenced by the relatively constant strain energy density with increasing mass. Additionally, increases in apparent mineral density and bone area fraction are quadrant dependent in the proximal and distal epiphyses of the P1, and variable between trabecular and cortical bone compartments.

At the cross-sectional level, our measurement of total bone area growth rate in the diaphysis is the same as that reported by others in Thoroughbred horses (6.3 mm²/week, Fig. 5A), although our values of bone area are almost double those reported (Firth et al., 2011). Similarly, our measurements for bone mineral density in the mid-diaphysis are comparable in value and have similar growth trends (Fig. 5B) (Firth et al., 2011). While some interbreed differences are expected in terms of absolute mass and size of the animal, the similarity in bone development rates between Thoroughbreds and Standardbred horses indicates a level of consistency in proximal phalanx development between breeds. This finding is supported by breed history, as the Thoroughbred is a foundation breed for the Standardbred, meaning all Standardbreds share genetic background with Thoroughbreds (StandardbredCanada, 2019).

Studies in Thoroughbreds have shown that most simple fractures to the proximal phalanx start on the lateral side of the sagittal groove (Ellis et al., 1987), in the lateral quadrant of the proximal epiphysis. Importantly, we found that apparent mineral density and bone area fraction accrual in Standardbreds are quadrant-dependent in the proximal and distal epiphyses, with the medial quadrant experiencing the most change during growth (Figs. 3, 4). Due to a short neck relative to limb length, young foals typically spread their forelimbs out laterally in order to reach the ground to eat. This posture causes the medial aspects of the limbs to carry more load than the lateral aspects. Further, the medial aspect of equine forelimbs have a larger articulating surface compared to the lateral aspect, which may indicate increased load medially. During quiet standing, we found that strain energy density in the medial aspect of the proximal epiphysis was higher than the lateral aspect (data not shown), perhaps inducing the bone changes observed within the medial quadrant. Using strain gauges in vivo during trotting, Gross et al. (1992) reported that diaphyseal strain energy density was non-uniform in distribution and higher in the medial quadrant compared to the lateral quadrant. Together, these data suggest that the propensity to fracture on the lateral aspect may be due to the relatively low cortical bone fraction and decreased degree of mineralization compared to the medial aspect.

The strain energy density in the diaphysis was constant as mass increased, indicating adaptation to the standing loading condition by having more mineralized cortical bone and more cortical bone area fraction than the distal or proximal epiphyses (Fig. 2). Changes in mineral density and bone area fraction in the diaphysis were similar in all quadrants, particularly in the cortical compartment. In contrast, the

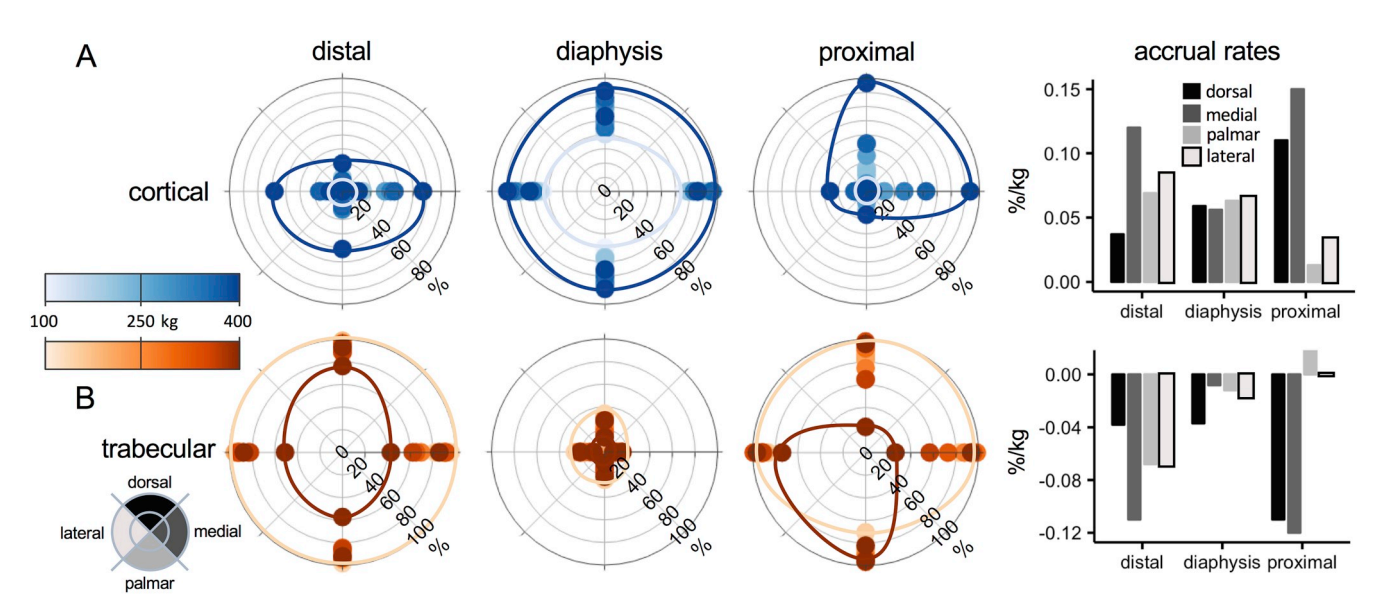


Fig. 4. Bone area fraction percentages in quadrants of the proximal phalanx bone for (A) cortical and (B) trabecular bone. Bone area fraction in % is plotted on the radial axis of the polar plots. Blue points represent cortical data, while orange points represent trabecular data. The lightly shaded lines indicate the data at 120 kg, while the darker shaded lines indicate the data at 382 kg. Evaluating the gap between these lines gives one an idea of growth in specific quadrants. Bar plots represent the accrual rates (change in bone area fraction/change in mass) for each quadrant. Columns are (left to right): distal epiphysis, diaphysis, proximal epiphysis, accrual rates.

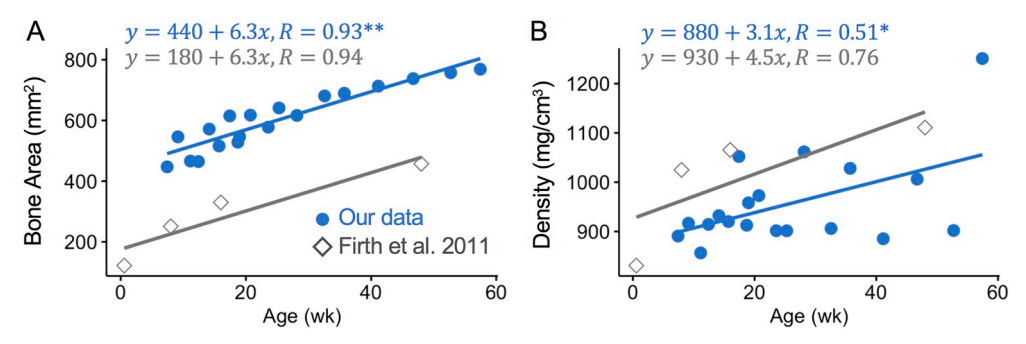


Fig. 5. Comparison of data for the proximal phalanx diaphysis from the present study and Firth et al. (2011) for (a) bone area and (b) density.

SED in both the distal and proximal epiphyses increased during growth indicating a lower level of adaptation to the quiet stance loading condition. Of note is that while the epiphyseal strain energy increased during growth, it is still likely below a fracture energy level. The increase in strain energy may be due to decreased mineralization levels of cortical bone in the epiphyses, but this remains to be determined as our results may be affected by the partial volume effect of our computed tomography data. Our data suggest that increased cortical mineralization and bone area fraction lowers diaphyseal SED during quiet standing condition. However, this hypothetical mechanism is not apparent in the epiphyses where trabecular bone is needed to dissipate energy and transfer joint loads to cortical bone in the diaphysis (Oftadeh et al., 2015). Increasing the amount and/or density of cortical bone in the epiphyses might stiffen the epiphyses and increase the likelihood of fracture

Our observations that foals spend little time moving faster than a walk may mean that any exercise intervention could benefit equine bone during post-natal development. It has been shown that mild exercise at an early age in horses is beneficial for bone development (Firth et al., 2011) and has no negative effects on subchondral bone (Dykgraaf et al., 2008), articular cartilage (Dykgraaf et al., 2008; van Weeren et al., 2008), or flexor tendon development (Moffat et al., 2008). Sagittal plane running may not be sufficient since gait patterns tend to preferentially load the medial aspect of the forelimb (Gross et al., 1992). Increasing the speed of exercise generally increases the magnitude of the load on the bone but does not greatly alter the loading direction (Biewener et al., 1983).

The optimal exercise intervention for inducing adaptation in what seems to be the weaker lateral aspect of the proximal phalanx would require increased lateral mechanical stimulus. Lateral loading can be induced by prescribing turning-based exercises. Tight turns, such as figure-eights, performed at speed must be used with caution to prevent soft tissue injury to the developing musculoskeletal system. To our knowledge, the effects of turning-based exercise interventions on equine bone and soft tissue development have not been studied. Firth et al. (2011) used an exercise intervention that included running laps on an oval track in alternating directions, but did not include analyses of the proximal epiphysis of the P1. Our data suggests that bone growth and adaptation in the P1 bone is spatially specific and best assessed on a functional quadrant basis, as averaging results across an entire cross-section can obscure important findings. Future exercise interventions should take care to evaluate bone adaptation at multiple locations of the P1 bone, including the proximal epiphysis.

While this study presents the first longitudinal assessment of equine bone properties during growth, it is not without limitations. Our sample size was limited to three subjects; however, all but four of the linear regressions were significant lending confidence in our characterization of normal development of the left proximal phalanx bone in Standardbred foals. Our analysis is bolstered by the use of mass as an independent variable which minimizes age-related size differences. The use of clinical quality CT data is an unavoidable limitation for a longitudinal *in vivo*

study in this species, and the in-plane voxel dimensions may lead to an underestimate of cortical bone area in the epiphyses through partial volume effect if cortical thickness is smaller than one voxel.

5. Conclusion

In summary, this work provides a baseline longitudinal characterization of normal modeling of the equine forelimb P1 during the first year of life and its effect on strain energy density - a biomechanical metric of potential bone remodeling. This information is an essential prerequisite to making evidence-based recommendations for training regimens that may encourage bone growth in areas prone to fracture during development. A properly prepared musculoskeletal system may lead to fewer fractures, thus reducing the unnecessary wastage of equine athletes.

Declaration of competing interest

The authors declare that they have no known competing financial interests or personal relationships that could have appeared to influence the work reported in this paper.

CRediT authorship contribution statement

Sara G. Moshage: Methodology, Software, Formal analysis, Investigation, Writing - original draft, Writing - review & editing. Annette M. McCoy: Methodology, Resources, Writing - review & editing, Funding acquisition. John D. Polk: Conceptualization, Resources, Funding acquisition, Writing - review & editing. Mariana E. Kersh: Conceptualization, Methodology, Writing - review & editing, Supervision, Funding acquisition.

Acknowledgements

We are grateful to Hyunggwi Song and Ida Ang for their assistance in code development, to Amy Narotsky for her assistance with data collection, and the staff of the UIUC Horse Farm and College of Veterinary Medicine. This work was supported by the University of Illinois Campus Research Board, Companion Animal Research Fund from the College of Veterinary Medicine at the University of Illinois at Urbana-Champaign, and the National Science Foundation (NSF-1639756). The funding sources had no involvement in study design, data analysis, or manuscript preparation.

Appendix A. Supplementary data

Supplementary data to this article can be found online at https://doi. org/10.1016/j.jmbbm.2019.103568.

References

Back, W., Clayton, H., 2013. Equine Locomotion, second ed. Elsevier, Edinburgh.

- Bertuglia, A., Bullone, M., Rossotto, F., Gasparini, M., 2014. Epidemiology of musculoskeletal injuries in a population of harness Standardbred racehorses in training. BMC Vet. Res. https://doi.org/10.1186/1746-6148-10-11.
- Biewener, A., Bertram, J., 1993. Mechanical loading and bone growth in vivo. Bone 7, 1–36
- Biewener, A.A., 1982. Bone strength in small mammals and bipedal birds: do safety factors change with body size? J. Exp. Biol. 98 (1), 289. LP 301. URL: http://jeb.biologists.org/content/98/1/289.abstract.
- Biewener, A.A., Thomason, J., Goodship, A., Lanyon, L.E., 1983. Bone stress in the horse forelimb during locomotion at different gaits: a comparison of two experimental methods. J. Biomech. 16 (8), 565–576. https://doi.org/10.1016/0021-9290(83) 90107-0. URL: http://www.sciencedirect.com/science/article/pii/00219290839 01072
- Dykgraaf, S., Firth, E.C., Rogers, C.W., Kawcak, C.E., 2008. Effects of exercise on chondrocyte viability and subchondral bone sclerosis in the distal third metacarpal and metatarsal bones of young horses. Vet. J. 178 (1), 53–61. https://doi.org/ 10.1016/j.tvjl.2007.08.016. URL: http://www.sciencedirect.com/science/article/ pii/\$1090023307002961.
- Ellis, D.R., Simpson, D.J., Greenwood, R.E.S., Crowhurst, J.S., 1987. Observations and management of fractures of the proximal phalanx in young Thoroughbreds. Equine Vet. J. 19 (1), 43–49. https://doi.org/10.1111/j.2042-3306.1987.tb02579.x.
- Ely, E.R., Avella, C.S., Price, J.S., Smith, R.K.W., Wood, J.L.N., Verheyen, K.L.P., 2009. Descriptive epidemiology of fracture, tendon and suspensory ligament injuries in National Hunt racehorses in training. Equine Vet. J. 41 (4), 372–378. https://doi. org/10.2746/042516409X371224. URL: http://www.ncbi.nlm.nih.gov/pubmed/19562899.
- Firth, E.C., Rogers, C.W., van Weeren, P.R., Barneveld, A., McIlwraith, C.W., Kawcak, C. E., Goodship, A.E., Smith, R.K.W., 2011. Mild exercise early in life produces changes in bone size and strength but not density in proximal phalangeal, third metacarpal and third carpal bones of foals. Vet. J. 190 (3), 383–389. https://doi.org/10.1016/j.tvjl.2010.11.016. URL: http://www.sciencedirect.com/science/article/pii/S109002331000403X.
- Frost, H., 1987. Bone "mass" and the "mechanostat": A proposal. Anatomical Record 219, 1–9. https://doi.org/10.1002/ar.1092190104.
- Georgopoulos, S.P., Parkin, T.D.H., 2017. Risk factors for equine fractures in Thoroughbred flat racing in North America. Prev. Vet. Med. 139, 99–104. https://doi.org/10.1016/j.prevetmed.2016.12.006.
- Gross, T.S., McLeod, K.J., Rubin, C.T., 1992. Characterizing bone strain distributions in vivo using three triple rosette strain gages. J. Biomech. 25 (9), 1081–1087. https:// doi.org/10.1016/0021-9290(92)90044-2. URL: http://www.sciencedirect.com/science/article/pii/0021929092900442.
- Harrison, S.M., Whitton, R.C., Kawcak, C.E., Stover, S.M., Pandy, M.G., 2010. Relationship between muscle forces, joint loading and utilization of elastic strain energy in equine locomotion. J. Exp. Biol. 213, 3998–4009. https://doi.org/ 10.1242/jeb.044545.
- Harrison, S.M., Whitton, R.C., Kawcak, C.E., Stover, S.M., Pandy, M.G., 2014. Evaluation of a subject-specific finite-element model of the equine metacarpophalangeal joint under physiological load. J. Biomech. 47, 65–73.
- Kersh, M.E., Martelli, S., Zebaze, R., Seeman, E., Pandy, M.G., 2018. Mechanical loading of the femoral neck in human locomotion. J. Bone Miner. Res. 33 (11), 1999–2006. https://doi.org/10.1002/jbmr.3529.
- Les, C., Keyak, J., Stover, S., Taylor, K.T., Kaneps, A.J., 1994. Estimation of material properties in the equine metacarpus with use of quantitative computed tomography. J. Orthop. Res. 12 (6), 822–833.
- McCarty, C.A., Thomason, J.J., Gordon, K.D., Burkhart, T.A., Milner, J.S., Holdsworth, D. W., 2016. Finite-element analysis of bone stresses on primary impact in a large-animal model: the distal end of the equine third metacarpal. PLoS One 11 (7). https://doi.org/10.1371/journal.pone.0159541.
- Moffat, P.A., Firth, E.C., Rogers, C.W., Smith, R.K.W., Barneveld, A., Goodship, A.E., Kawcak, C.E., McIlwraith, C.W., R, v.W.P., 2008. The influence of exercise during growth on ultrasonographic parameters of the superficial digital flexor tendon of young Thoroughbred horses. Equine Vet. J. 40 (2), 136–140. https://doi.org/10.2746/042516408X253109. URL:
- Oftadeh, R., Perez-Viloria, M., Villa-Camacho, J.C., Vaziri, A., Nazarian, A., 2015. Biomechanics and mechanobiology of trabecular bone: a review. J. Biomech. Eng. 137 (1) https://doi.org/10.1115/1.4029176. URL:
- O'Hare, L.M.S., Cox, P.G., Jeffery, N., Singer, E.R., 2013. Finite element analysis of stress in the equine proximal phalanx. Equine Vet. J. 45 (3), 273–277. https://doi.org/10.1111/j.2042-3306.2012.00635.x.

- Parkin, T.D.H., Clegg, P.D., French, N.P., Proudman, C.J., Riggs, C.M., Singer, E.R., Webbon, P.M., Morgan, K.L., 2004. Race- and course-level risk factors for fatal distal limb fracture in racing Thoroughbreds. Equine Vet. J. 36 (6), 521–526. https://doi. org/10.2746/0425164044877332.
- Parkin, T.D.H., Clegg, P.D., French, N.P., Proudman, C.J., Riggs, C.M., Singer, E.R., Webbon, P.M., Morgan, K.L., 2004. Risk of fatal distal limb fractures among thoroughbreds involved in the five types of racing in the United Kingdom. Vet. Rec. 154 (16), 493–497. https://doi.org/10.1136/vr.154.16.493.
- Prendergast, P.J., Taylor, D., 1994. Prediction of bone adaptation using damage accumulation. J. Biomech. 27 (8), 1067–1076. https://doi.org/10.1016/0021-9290 (94)90223-2. URL: http://www.sciencedirect.com/science/article/pii/002192909 4902232
- Riggs, C.M., 2002. Fractures a preventable hazard of racing thoroughbreds? Vet. J. 163 (1), 19–29. https://doi.org/10.1053/tvjl.2001.0610.
- Rogers, C.W., Firth, E.C., McIlraith, C.W., Barneveld, A., Goodship, A.E., Kawcak, C.E., Smith, R.K.W., van Weeren, P.R., 2008. Evaluation of a new strategy to modulate skeletal development in racehorses by imposing track-based exercise during growth: the effects on 2- and 3-year-old racing careers. Equine Vet. J. 40 (2), 119–127. https://doi.org/10.2746/042516408X266088. URL:
- Ruff, C., Holt, B., Trinkaus, E., 2006. Who's afraid of the big bad Wolff?: "Wolff's law" and bone functional adaptation. Am. J. Phys. Anthropol. 129 (4), 484–498. https://doi.org/10.1002/ajpa.20371. URL:
- Schindelin, J., Arganda-Carreras, I., Frise, E., Kaynig, V., Longair, M., Pietzsch, T., Preibisch, S., Rueden, C., Saalfeld, S., Schmid, B., Tinevez, J.Y., White, D.J., Hartenstein, V., Eliceiri, K., Tomancak, P., Cardona, A., 2012. Fiji: an open-source platform for biological-image analysis. Nat. Methods 9, 676. https://doi.org/10.1038/nmeth.2019 {#}supplementary-information. http://10.0.4.14/nmeth.2019. https://www.nature.com/articles/nmeth.2019.
- Smallwood, J.E., Albright, S.M., Metcalf, M.R., Thrall, D.E., Harrington, B.D., 1989.
 A xeroradiograhic study of the developing equine foredigit and metacarpophalangeal region from birth to six months of age. Vet. Radiol. 30 (3), 98–110. https://doi.org/10.1111/j.1740-8261.1989.tb00753.x.
- StandardbredCanada, 2019. History of the standardbred. URL: https://standardbredcanada.ca/content/new-racing-history-standardbred.html.
- Strand, E., Braathan, L., Hellsten, M., Huse-Olsen, L., Bjornsdottir, S., 2007. Radiographic closure time of appendicular growth plates in the Icelandic horse. Acta Vet. Scand. 49 (19).
- Swanstrom, M.D., Stover, S.M., Hubbard, M., Hawkins, D.A., 2004. Determination of passive mechanical properties of the superficial and deep digital flexor muscleligament-tendon complexes in the forelimbs of horses. Am. J. Vet. Res. 65 (2), 188–197. URL: https://avmajournals.avma.org/doi/pdf/10.2460/ajvr.2004.65.188.
- 188–197. URL: https://avmajournals.avma.org/doi/pdt/10.2460/ajvr.2004.65.188.
 Turley, S., Thambyah, A., Riggs, C., Firth, E., Broom, N., 2014. Microstructural changes in cartilage and bone related to repetitive overloading in an equine athlete model.
 J. Anat. 224 (6), 647–658.
- Verheyen, K.L.P., Wood, J.L.N., 2004. Descriptive epidemiology of fractures occurring in British Thoroughbred racehorses in training. Equine Vet. J. 36 (2), 167–173. https://doi.org/10.2746/0425164044868684.
- Warden, S.J., Hurst, J.A., Sanders, M.S., Turner, C.H., Burr, D.B., Li, J., 2005. Bone adaptation to a mechanical loading program significantly increases skeletal fatigue resistance. J. Bone Miner. Res. 20 (5), 809–816. https://doi.org/10.1359/ JBMR_041222_URL:
- Warden, S.J., Mantila Roosa, S.M., Kersh, M.E., Hurd, A.L., Fleisig, G.S., Pandy, M.G., Fuchs, R.K., 2014. Physical activity when young provides lifelong benefits to cortical bone size and strength in men. Proc. Natl. Acad. Sci. 111 (14), 5337. https://doi.org/10.1073/pnas.1321605111. LP 5342. URL: http://www.pnas.org/content/111/14/5337.abstract.
- van Weeren, P.R., Firth, E.C., Brommer, H., Hyttinen, M.M., Helminen, H.J., Rogers, C. W., DeGroot, J., Brama, P.A.J., 2008. Early exercise advances the maturation of glycosaminoglycans and collagen in the extracellular matrix of articular cartilage in the horse. Equine Vet. J. 40 (2), 128–135. https://doi.org/10.2746/042516408X253091. URL:
- Weller, R., Pfau, T., May, S.A., Wilson, A.M., 2006. Variation in conformation in a cohort of National Hunt racehorses. Equine Vet. J. 38 (7), 616–621. https://doi.org/ 10.2746/042516406X150394. URL:
- Zysset, P., Dall'Ara, E., Varga, P., Pahr, D., 2013. Finite element analysis for prediction of bone strength. BoneKEy Rep. 2, 386.